Journal of Sound and Vibration 329 (2010) 4656–4671

Contents lists available at ScienceDirect

Journal of Sound and Vibration

journal homepage: www.elsevier.com/locate/jsvi

On the non-linear dynamic behavior of elastohydrodynamic lubricated point contact

Fábio Nonato [a], Katia L. Cavalca [b,*]

[a] Schaeffler Brasil Ltda, 3500-A Independência Avenue, 18087-101 Sorocaba SP, Brazil
[b] Department of Mechanical Design, Unicamp, Postal Box 6122, 13083-970 Campinas SP, Brazil

ARTICLE INFO

Article history:
Received 31 March 2010
Accepted 17 May 2010
Handling editor: H. Ouyang
Available online 15 June 2010

ABSTRACT

The complex dynamic concepts of mechanical systems are regarded each day as new barriers to be overcome. One of the most complex systems, despite its common construction design, is the rolling element bearings. The interactive dynamic interfaces of such bearings are normally disregarded by engineering analysis on the day to day basis due to its complexities. This paper intends to propose a new approach to the characterization of the elastohydrodynamic lubricated point contacts on such components, in order to fully depict its non-linear dynamic behavior, avoiding the use of rough hypothesis on a systemic procedure. A multi-level method was used to solve the coupled lubrication–deformation problem, alongside a Newmark-ß integrator of the motion equation for the contact system. A range of dynamically similar contacts were evaluated, so as to characterize its nonlinear dynamic behavior. A least-squares method was applied to the multi-level algorithm results, fitting the displacements–force relation to a linear and also to a third order polynomial stiffness. The fitting results were compared, clearly showing the nonlinear behavior of such contacts. Also, the oil film damping was regarded as viscous, leading to good overall response. Some peculiarities of the proposed adjust method are also considered.

1. Introduction

The time reduction between product updates and new developments in the mechanical industries brings new challenges to the development team. Old assumptions and rough concepts can mislead the project and increase the number of practical experiments needed. Working with prototypes or finished products experimentally is a great engineering tool to understand systemic behavior. Also, methods like DOE and accelerated testing can decrease the total experimentation phase time. However, the only way to overcome the time issue is to reduce the chances of a prototype go wrong. Using the right simulation tools and methods, the development group can provide better parts, or in some cases, even finished parts, without extensive bench tests ever occur. So, the need for better mechanical models is the first to arise.

Dealing with complex dynamic systems is a common procedure in the industries nowadays. For those cases, even now, some rough modeling hypotheses are used, and the problem itself is not very well represented. That is the case of rolling element bearings.

That kind of machine element usually has failure issues related to vibration and noise, which arise from problems such as pitting and spalling. Those events are directly related to the contact forces acting between components and the associated contact fatigue. Thus, it is essential to understand those conditions in order to increase bearing life and quality.

* Corresponding author. Tel.: +55 19 3521 3178; fax: +55 19 3289 3722.
E-mail addresses: paulafbi@schaeffler.com (F. Nonato), katia@fem.unicamp.br (K.L. Cavalca).

0022-460X/$ - see front matter © 2010 Elsevier Ltd. All rights reserved.
doi:10.1016/j.jsv.2010.05.014

Nomenclature

a	contact ellipse minor semi-axis [m]
A_h	harmonic excitation amplitude
B_4	mixed dynamic coefficient
C_i	damping coefficient of the ith order
E	second order elliptic integral
f_d	dynamic contact force
$H(X, Y)$	dimensionless film thickness
H_c	dimensionless central film thickness
H_{min}	dimensionless minimal film thickness
H_0	dimensionless mutual approach
K_i	stiffness coefficient of the ith order
K	first order elliptic integral
L	Moes dimensionless parameter
m	rolling element mass [g]
M	Moes dimensionless parameter
p_n	Hertz contact pressure [Pa]
P	dimensionless pressure
R	curvature sum [1/m]
R_X	curvature sum in the X direction [1/m]
R_Y	curvature sum in the Y direction [1/m]
e_v	fitting residual for v variable
S	dimensionless geometric parameter
T	dimensionless time
u	principal variable of the mechanical system, position
$\dot{u}$	velocity of the mechanical system
$\ddot{u}$	acceleration of the mechanical system
u_m	sum of surfaces velocities [m/s]
X	dimensionless longitudinal direction
Y	dimensionless transversal direction
η_0	viscosity at amb. pressure [N s/m^2]
$\overline{\eta}$	viscosity ratio
κ	contact elliptic ratio
$\overline{\lambda}Z$	dimensionless Reynolds equation parameter
v	Poisson's ratio
$\overline{\rho}$	density ratio
Ω_n	dimensionless natural frequency
Ω_e	dimensionless excitation frequency

The rolling elements bearings, due to its periodical geometrical nature, are a vibration source themselves. In order to fully understand the complexities of the dynamic behavior of rolling elements bearings, its basic functional characteristics must be studied, the mechanical contacts linking its elements and the raceways. Those contacts are the only vibration transmission points between the shaft inside the bearing and bearing housing.

The first studies on the properties of these contacts were made by H. R. Hertz and published on the work "Über die Berührung fester elasticher Körper". Due to this work, the general contact mechanics of elastic bodies was named after Hertz. Directly from his work, the nonlinear behavior of the contact can be attained.

The direct use of the dry contact stiffness, as presented in [1], can be a useful approximation to the dynamics of the full bearing, but, doing so, the lubricant effects are neglected. Since the first studies on the lubrication of highly loaded contacts, the damping and stiffness of the oil film are known to be effective over the contact. Due to the influence of the elastic deformation on the oil film thickness this type of lubrication was entitled Elastohydrodynamic (EHL).

The first satisfactory numerical results for the point EHL contact were presented by Hamrock in [2]. In his work, a finite difference method was used for the steady state lubricated problem, using a Gauss-Seidel iterative method. But there was not until great improvement on the computational power and the use of advanced methods that the transient EHL contact could be analyzed.

In the 80s and 90s there were multiple successful attempts to introduce a robust numerical method to evaluate the EHL static condition. Evans and Snidle [3,4] proposed a quasi-inverse method to solve heavily loaded point contacts, as the previous Gauss-Seidel iterative schemes were not sufficiently robust for that matter. The method was based on the inverse solution employed by Dowson and Higgins for the line contact problem.

Also the substitution of the Gauss-Seidel iterative scheme by a Newton–Raphson method was investigated by Park and Kim [5] to overcome the high computational costs of such procedure. However, even with the low dependence of the convergence on the relaxation factors, the Newthon–Raphson method is highly dependent on the initial guess; in this case, of the pressure and thickness distributions.

In 1991, Venner introduced the multi-level method for the EHL point contact, using the multi-level multi-integration, MLMI, to evaluate the elastic deformation due to the high contact pressure (Venner and Ludbrecht, [6]).

Based on a set of meshes with different grid sizes, this method can greatly reduce computational time by operating the different error frequencies components on different discretization grids. The multiple grid approach reduces dramatically the computational costs and to overcome the high load convergence problem, a hybrid relaxation method is used, adding the Jacobi relaxation method to evaluate high pressure zones. Anyhow, a finite difference method is used to evaluate the Reynolds equation on those grids.

Most of the developments on the transient EHL contacts afterwards were in the surface discontinuities field. In [7] and [8], the effect of surface topology was evaluated as a moving transverse ridge through the contact or as waviness of the surface.

Using this improved method, Wijnant first demonstrate the transient contact response due to harmonic excitation and free vibration in [9]. In his work, the influence of the transient response is observed over the film thickness and most of all the first linear fit of the dynamic response is introduced, achieving the first simulated values for the oil damping on EHL contacts.

Using these fitted values of damping and stiffness coefficients, Wensing [10] observed the influence of the rolling element bearing on a simple rotor system. Also in Wijnant and Wesing [11], some comments on the contact dynamics can be found. Some improvements on the transient EHL algorithm were also proposed by Goodyer [12], focused on an algorithm optimization and studying some surface topology problems. However, no present models for the contact force of lubricated point contacts is robust enough to be incorporated in a full bearing model, as the use of linear springs can be misleading and misinterpret some of the oil film behaviors. For instance, the predicted mutual approach has an asymmetric behavior with respect to the equilibrium position; hence no linear spring can contemplate such peculiarity.

The first attempts to simulate a transient non-linear model of the EHL contacts were made by Nonato and Cavalca [13], using a least square method to fit the transient response of a circular EHD contact. In this work, the same approach will be taken to evaluate the transient and harmonic responses of elliptic EHL contacts. Both results will be compared, in order to fully understand the behavior of the fitting methods. Also, the use of transient and harmonic responses from identical contacts parameters should give a quite trustful method to verify the EHL dynamic simulations. At the end, both methods are supposed to have similar behavior and shall dynamically describe the predicted lubricant film behavior.

A trustful EHL contact dynamic force model is a significant step on having the full rolling element bearing model, regarding the lubricant forces equilibrium. Consequently, the bearing model could be validated against real rolling element bearings on a straightforward Jeffcot rotor test bench, as the validation of such transient contacts are of great complexity. Therefore, this first-hand methodology complies with the necessities for a robust contact model applied to the full bearing dynamic system, avoiding any misleading interpretation of the predicted film, due to a direct linearization of the contact.

The main objective of this paper is to introduce a more reliable lubricated contact force model, based on the predicted film behavior of the EHL transient multi-level algorithm. Hereafter, allowing a future validation of the full lubricated rolling element bearing model on rotor dynamics.

2. EHL dynamic model

A multi-level algorithm as presented in Venner and Ludbrecht [6] and adapted to the transient elliptic load, as in Wijnant [9], was used to model the dynamic EHL problem. The fluid flow was evaluated using the Reynolds equation for a gap flow, with the squeeze term. The dimensionless form of the Reynolds equation is shown in Eq. (1).

$$\frac{\partial}{\partial X}\left(\frac{\overline{\rho}H^3}{\overline{\eta}\overline{\lambda}}\frac{\partial P}{\partial X}\right)+\kappa^2\frac{\partial}{\partial Y}\left(\frac{\overline{\rho}H^3}{\overline{\eta}\overline{\lambda}}\frac{\partial P}{\partial Y}\right)-\frac{\partial(\overline{\rho}H)}{\partial X}-\frac{\partial(\overline{\rho}H)}{\partial T}=0 \tag{1}$$

In this case, H and $P$are, respectively, the dimensionless film thickness and pressure, $\overline{\eta}$ and $\overline{\rho}$ are the fluid properties, κ^2 is the contact elliptic ratio, given by the contact geometry, and $\overline{\lambda}$ is a dimensionless group given by

$$\overline{\lambda}=\frac{6u_m\eta_0(2R)^2}{a^3p_h}\left(\frac{\mathrm{E}}{\mathrm{K}}\right)^2 \tag{2}$$

Along with the Reynolds equation, the elastic integral has to be solved for the contact strain. The thickness equation reads

$$H(x,y)=H_0+SX^2+(1-S)Y^2+\frac{1}{\mathrm{K}\pi}\int_{-\infty}^{\infty}\int_{-\infty}^{\infty}\frac{P(X',Y')dX'dY'}{\sqrt{(Y-Y')^2+\kappa^2(X-X')^2}} \tag{3}$$

where the fourth term on the right hand side is the deformation integral, the second and third terms are the geometrical approximation for the elliptic body and the first term is the mutual approach of the bodies. Due to the transform integral nature of this equation, special care must be taken. The MLMI method, as in Venner and Ludbrecht [6], was applied to evaluate such integral. With respect to the elliptic ratio κ, the corrections in both directions must be adjusted proportionally, when evaluating the discontinuity at $Y=Y'$ and $X=X'$.

In opposition to the surface topology evaluations, the principal variable is the mutual approach. This variable represents the relative movement of two non-deformed points of the contacting bodies, against each other. Thus, the dynamic behavior of the rolling element against a fixed raceway can be evaluated. The mutual approach, in the static condition, is obtained from the force balance equation as the integral constant.

$$\frac{3}{2\pi}\int_{-\infty}^{\infty}\int_{-\infty}^{\infty}P(X,Y)dX\,dY=1 \tag{4}$$

For the transient case, an equation of motion is needed. So, as presented in Wijnant [9] and reproduced by Goodyer [12], the inertia term, related to the mass of the rolling element, is introduced in a dimensionless natural frequency approach, as in Eq. 5.

$$\frac{1}{\boldsymbol{\Omega}_n^2}\frac{d^2H_0}{dT^2}+\frac{3}{2\pi}\int_{-\infty}^{\infty}\int_{-\infty}^{\infty}P(X,Y,T)dX\,dY=1 \tag{5}$$

where $\Omega_n^2=(8fRE)/(mu_mK)$ is the dimensionless natural frequency. Eq. 5 represents the free vibration mode of the system. In order to solve this second order differential equation two initial conditions must be employed, one in the displacement and one in the velocity. Physically, introducing a displacement or velocity condition is a hard goal to achieve, as the contacting bodies are rotating. But numerically, such an approach is the most feasible one.

To avoid the use of non-realistic initial conditions to obtain the transient response, the harmonic excitation can be applied. As stated by Wijnant [9], the influence of the inertia term tends to be small, due to the $1/\Omega_n^2$ factor. Thus, assuming a greater influence of the load term, in a harmonic loading condition, the movement equation can be rewritten as in Wijnant [9]

$$\frac{3}{2\pi}\int_{-\infty}^{\infty}\int_{-\infty}^{\infty} P(X, Y, T)dX\,dY = 1+A_h\sin(\Omega_e T) \tag{6}$$

where Ω_e is the excitation frequency and A_h the amplitude. Eq. (6) is applicable mostly in a quasi-static approach, assuming that the speed of changes in the contact is greater than the speed of the changes in the load, i.e., $\Omega_n \gg \Omega_e$. In other words, the changes in the oil film stabilize fast enough not to influence the harmonic response.

Also the pressure dependent relations of the fluid properties have to be evaluated with the transient model. The Dowson and Higgins [14] density–pressure relation and the Roelands equation for the viscosity–pressure relation, as presented in Larsson [15], were applied.

2.1. Linear dynamic model

Considering the oil film as a set of linear spring and damper, the EHL contacts become a linear dynamic system. Fig. 1 shows this simplified model of the problem, as initially proposed by Wijnant and Wensing [11].

This simple approach is very useful to understand the complete bearing dynamic system. Previously, when dealing only with the dry contact model, the same situation occurs, only without the damping, provided by the oil film, and the stiffness being the one from the Hertzian contact model.

In this case, the equation of motion can be rewritten as

$$\frac{1}{\Omega_n^2}\frac{d^2H_0}{dT^2}+C_1\frac{dH_0}{dT}+K_1H_0=1 \tag{7}$$

The contact forces generated at the inner and outer raceways contacts are adjusted to a set of stiffness and damping coefficients, given by K_1 and C_1. As seen before, the dimensionless contact force is given by the integral of the pressure over the contact area. This force, acting on the contacts, is the total force of the contact system, thus it balances both transient and harmonic movement equations. For the sake of simplicity, the mutual approach H_0 will be replaced by u, as the principal variable. So, for the dimensionless contact force, one might have

$$K_1u+C_1\dot{u}=\frac{3}{2\pi}\int_{-\infty}^{\infty}\int_{-\infty}^{\infty} P(X, Y, T)dX\,dY=f_d \tag{8}$$

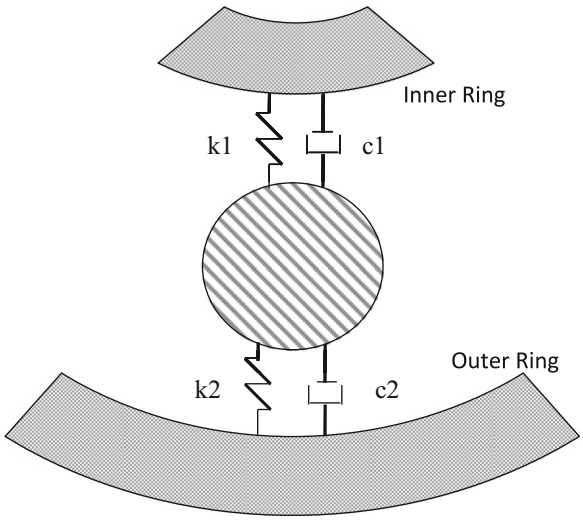

Fig. 1. Approximated spring and damper linear model.

In Wijnant [9], the stiffness and damping coefficients of the linear dynamic model were obtained by an implicit method, as the mutual approach is a function of the applied load. But the relation can be treated only in the dimensional form, therefore a particular contact characterized only by the dimensionless contact parameters cannot be evaluated without assuming some physical values.

The damping coefficient is obtained by the integration of the ellipse created by the $f_d \times H_0$ function. The total amount of energy absorbed by the fluid film is equal to the area of the ellipse. In this case, the coefficient can easily be found using only the dimensionless results.

In order to simplify the fitting procedures a least-square method can be used to approximate the evaluated forces to the dynamic model. Therefore, as in Eq. (8), the difference between the dynamic contact force, f_d, and the supposed linear dynamic model has to be minimized in order to obtain the coefficients. The total force and the values for displacement and velocity are calculated at each time-step using the EHL dynamic model.

Defining the squared quantity q^2 as the difference between f_d and the hypothetical linear system, at each simulated time-step, w, one might have

$$q^2 = \sum_{w=0}^{N} ((f_d)_w - K_1 u_w - C_1 \dot{u}_w)^2 \tag{9}$$

Minimizing the relation for K_1 and C_1, the following linear system can be achieved

$$\begin{bmatrix} \sum_{w=0}^{N} (u_w)^2 & \sum_{w=0}^{N} \dot{u}_w u_w \\ \sum_{w=0}^{N} \dot{u}_w u_w & \sum_{w=0}^{N} (\dot{u}_w)^2 \end{bmatrix} \begin{bmatrix} K_1 \\ C_1 \end{bmatrix} = \begin{bmatrix} \sum_{w=0}^{N} (f_d)_w u_w \\ \sum_{w=0}^{N} (f_d)_w \dot{u}_w \end{bmatrix} \tag{10}$$

Wijnant [9] used the harmonic vibration equation instead of the motion equation in order to obtain the dynamic coefficients. So as to compare the techniques, the least square method can also be applied to the harmonic equation. There is no need to rearrange the equations, as the same dynamic force has to be adjusted.

The least-square fitting method for the lubricant forces is commonly used in experimental methods for hydrodynamic bearings, as presented in Zhao [16], Zhou [17] and Castro [18]. However, the nonlinear form is commonly used, as the linear coefficients are acquired by other methods. The next section we introduce the nonlinear fitting process to the EHL case.

2.2. Nonlinear dynamic model

In the same way that the dynamic force in Eq. (8) can be adjusted to a linear spring and damper model, it can be adjusted to a nonlinear model, as proposed by Zhao [16] and Zhou [17] for the hydrodynamic lubricant film. In this case, only one direction is considered, i.e., the only possible motion is normal to the contact plane. Thus, the dynamic force is written as

$$f_d = K_1 u + C_1 \dot{u} + K_2 u^2 + C_2 \dot{u}^2 + K_3 u^3 + C_3 \dot{u}^3 + B_4 u\dot{u} \tag{11}$$

where B_4 is the mixed dynamic coefficient, depending on both velocity and displacement. Likewise, a linear system can be found minimizing the relation. The linear system is presented in Eq. (12).

$$\begin{bmatrix} \sum_{w=0}^{N} (u_w)^2 & \sum_{w=0}^{N} \dot{u}_w u_w & \sum_{w=0}^{N} (u_w)^3 & \sum_{w=0}^{N} (\dot{u}_w)^2 u_w & \sum_{w=0}^{N} (u_w)^4 & \sum_{w=0}^{N} (\dot{u}_w)^3 u_w & \sum_{w=0}^{N} (u_w)^2 \dot{u}_w \\ & \sum_{w=0}^{N} (\dot{u}_w)^2 & \sum_{w=0}^{N} (u_w)^2 \dot{u}_w & \sum_{w=0}^{N} (\dot{u}_w)^3 & \sum_{w=0}^{N} (u_w)^3 \dot{u}_w & \sum_{w=0}^{N} (\dot{u}_w)^4 & \sum_{w=0}^{N} (\dot{u}_w)^2 u_w \\ & & \sum_{w=0}^{N} (u_w)^4 & \sum_{w=0}^{N} (u_w)^2 (\dot{u}_w)^2 & \sum_{w=0}^{N} (u_w)^5 & \sum_{w=0}^{N} (u_w)^2 (\dot{u}_w)^3 & \sum_{w=0}^{N} (u_w)^3 \dot{u}_w \\ & & & \sum_{w=0}^{N} (\dot{u}_w)^4 & \sum_{w=0}^{N} (u_w)^3 (\dot{u}_w)^2 & \sum_{w=0}^{N} (\dot{u}_w)^5 & \sum_{w=0}^{N} (\dot{u}_w)^3 u_w \\ & \textit{symmetric} & & & \sum_{w=0}^{N} (u_w)^6 & \sum_{w=0}^{N} (u_w)^3 (\dot{u}_w)^3 & \sum_{w=0}^{N} (u_w)^4 \dot{u}_w \\ & & & & & \sum_{w=0}^{N} (\dot{u}_w)^6 & \sum_{w=0}^{N} (\dot{u}_w)^4 u_w \\ & & & & & & \sum_{w=0}^{N} (u_w \dot{u}_w)^2 \end{bmatrix} \begin{bmatrix} K_1 \\ C_1 \\ K_2 \\ C_2 \\ K_3 \\ C_3 \\ B_4 \end{bmatrix} = \begin{bmatrix} \sum_{w=0}^{N} (f_d)_w u_w \\ \sum_{w=0}^{N} (f_d)_w \dot{u}_w \\ \sum_{w=0}^{N} (f_d)_w (u_w)^2 \\ \sum_{w=0}^{N} (f_d)_w (\dot{u}_w)^2 \\ \sum_{w=0}^{N} (f_d)_w (u_w)^3 \\ \sum_{w=0}^{N} (f_d)_w (\dot{u}_w)^3 \\ \sum_{w=0}^{N} (f_d)_w \dot{u}_w u_w \end{bmatrix} \tag{12}$$

Solving the linear system leads to a solution vector with all dynamic coefficients. As seen in Eqs. (10) and (12), the system is symmetrical and can be easily evaluated by a straightforward computational method.

3. Numerical simulation

Along with the finite difference multi-level method for the evaluation of the Reynolds equation, a hybrid relaxation method was used as presented in Venner and Ludbrecht [6]. Both Gauss-Seidel and Jacobi models were used for the discretization of the problem. Even though the mesh dependent relaxation triggering value proposed, for choosing between models, produced fine values, making this a fixed value improves convergence on finer grids, as shown in Nonato [19].

The need for two relaxation procedures comes from the dual behavior of the problem. As can be seen in Eq. (1), when the pressure is high, i.e., inside the contact area, the viscosity ratio becomes extremely high and the equation is governed mostly by the advection operator. On the other hand, when the pressure is low, the Pouisseuille terms are more effective over the oil film flow.

As given in Wijnant [9], the dimensionless natural frequency of the EHL contact is related to the one in the dry hertzian contact. In that case, the period of oscillation is given by $T_n=5.13/\Omega_n$, so the values for the constant Ω_n was chosen to be 0.5, 1 and 2 times the dry contact frequency of 5.13, for most of the simulations. For the harmonic excitations, a $\Omega_e=n\,\pi$ relation was used, being n equal to 1.0, 2.0 and 4.0. The A_h exciting amplitude can be selected as a small percentage of the mean force, here to be 10%.

In order to characterize the EHL contact, the dimensionless parameters M and L introduced by Moes [20] were used. They are related to the imposed load and the lubricant parameters, respectively. Also is necessary to specify the elliptic ratio of the contact. As shown in Wijnant [9], as well as in Nonato [19], the effect of the elliptic ratio tends to decouple both directions in the Reynolds and thickness equations, leading to a result similar to one of lower load cases. In this paper, $\kappa=0.5$ was chosen to represent a mean value of an elliptic ratio.

The motion equation was evaluated using a Newmark-ß method. As the pressure is fully dependent on the integrated variable H_0, the discrete equation has to be analyzed during the relaxation of the Reynolds equation.

Both numerical verification and model validation were made based on previous results present on the vast EHL bibliography. The first direct verification of the multi-level model took into account the values of mutual approach presented by Wijnant [9]. Fig. 2 shows the simulated values of the mutual approach, along with the prediction functions, depicted with lines, from Wijnant [9]. The results are sufficiently close to the fitted prediction functions of Wijnant, as they are just a numerical fit to the actual simulation results. Therefore, both algorithms present the same results for the evaluated range of M and L.

In order to further validate the numerical model, the results obtained for a specific condition can be checked against previous experimental results. The same approach as in Wijnat [9] was used. A setup of a steel ball running against a glass disc with a thin Cr layer was used to simulate experimentally a lubricated contact. By means of the interference of the reflected beams from the Cr layer on the ones from the steel ball, a microscope can capture a fringe pattern arising from the light focused on the contact. Each of these fringes represents a level of more or less the same film thickness; therefore the shape of the oil film can be depicted. This procedure is commonly known as an interferometry analysis and it is the current, most common method to evaluate the thin EHL film between two surfaces. For more information on the interferometry procedures and methods, please refer to Wijnant [9] and Ren [21] and Chaomleffel [22].

Based on the experimental results present in Wijnant [9], the algorithm used to model the EHL contacts was validated. Firstly, the steady state contact was evaluated. The contact parameters are $M=58.07$, $L=4.62$ and $\Omega_n=2.4$. As the steel ball is pressed against a flat surface, the contact area is a circle, therefore $\kappa=1.0$. In this case, the basic algorithm is unaltered and

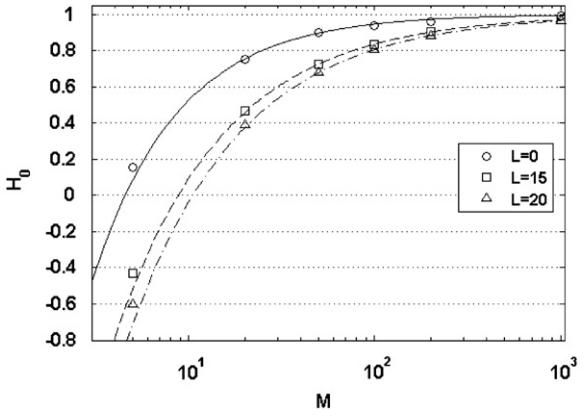

Fig. 2. Fitted mutual approach, H_0, as a function of M and $L=20$(– ● –), $L=15$ (– –) and $L=0$ (—).

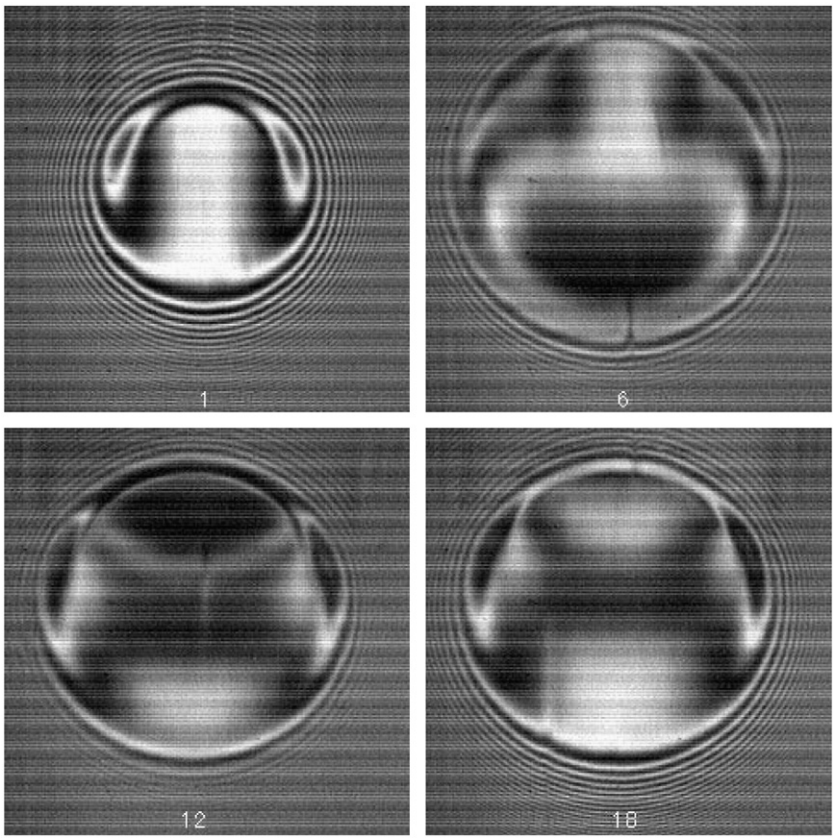

Fig. 3. Experimental interferograms obtained for, $0.0 \leq t \leq 4.0$ ms (Wijnant [9]).

the results can be directly compared. The measured minimum and central film thickness were $h_m^* = 0.15$ and $h_c^* = 0.34\,\mu m$. The calculated central film thickness, h_c=0.329 μm differs only 3% from the measured thickness; however, the minimum film thickness, h_c=0.187 μm differs approximately 20% from the measured one. Both results match the ones found by Wijnant [9].

For the transient case, however, the actual loading condition on the experiment should be modeled. Hence, some modifications to the algorithm must be made. The static loading condition is replaced by a ramp loading, which emulates the sudden impact loading imposed to the experimental test rig in order to excite the free vibration of the contact. Here, the dimensionless load increases linearly from 1.0 to 3.67 in a dimensionless time frame of 1.69. Fig. 3 shows the experimental interferograms for 0.0 to 4.0 ms reproduced from Wijnant [9]. The same time frames were obtained using the present algorithm. Fig. 4 depicts the pseudo-interferograms for the ramp load.

The correlation between both simulation and experimental data shows a fair agreement, as found by Wijnant [9]. However, as also stated by Wijnant [9], it is extremely difficult to investigate the influence of individual EHL contacts from measurements on full bearings. Hence, deriving a trustful theoretical model and subsequently incorporating these models in a full bearing dynamic enables to study its vibration behavior and noise effects. Such influence of the full bearing dynamic model over the system can be assessed on a coupled bearing rotor non-linear model as presented by Chang-Jian and Chen [23] for hydrodynamic bearings.

4. Dynamic results

Using the algorithm presented in Nonato [19], the EHL transient contacts were evaluated in order to obtain the contact displacement and velocity for a given period of time. Firstly, the free vibration model was evaluated for a particular case, with two different dimensionless natural frequencies Ω_n (2.56 and 5.13). The displacement results for the simulated examples are presented in Fig. 5.

The overall behavior of the responses was adequate, and also the film damping effect can be clearly observed in curves. At a first glance, the EHL contact system behaves basically as a linear stiffness and viscous damping mechanical 1 DOF system. But some care must be taken, as the basic contact model used for both the dry and the lubricated contact are basically non-linear. Deeper evaluation of these responses is made latter in this work.

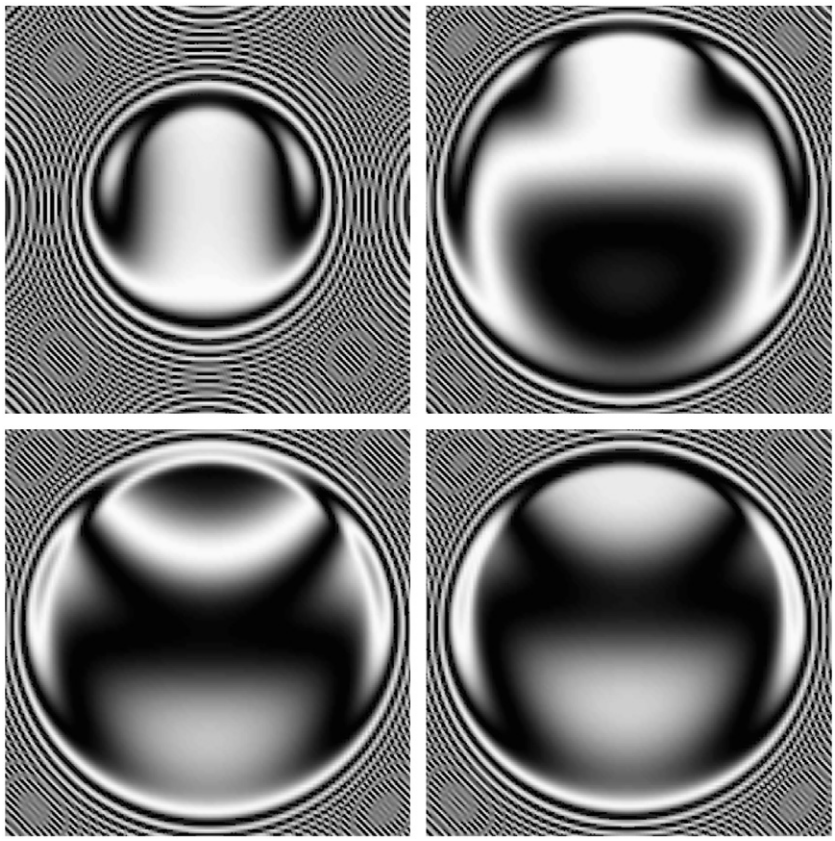

Fig. 4. Calculated pseudo-interferograms for ,$0.0 \leq t \leq 4.0$ ms, i.e., dimensionless $0.0 \leq T \leq 5.6$.

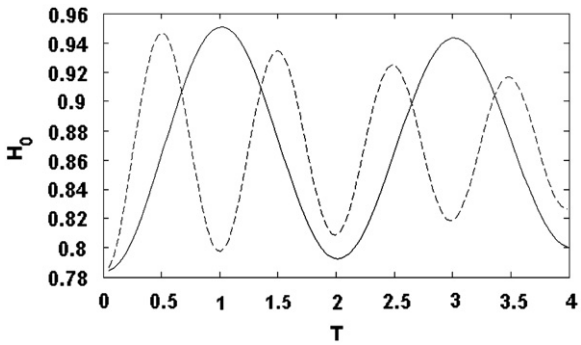

Fig. 5. Transient mutual approach response for EHL elliptic contact with M=200 and L=10 for two different natural frequencies, Ω_n=513 (– –) and Ω_n=256 (—).

Other common characteristic of the dynamic EHL contact is the wave propagation arising from the advection term on the Reynolds equation. In other words, any disturbance of the film thickness induced at any point propagates with the velocity of the film across the contact area. This can be observed in Fig. 6, where both the minimum film thickness and the central film thickness are plotted for the Ω_n=513 case.

An important characteristic for the central film thickness is that, initially, its value remains constant. Close to one dimensionless time unit, referred here as T, the first valley occurs. Therefore, with a constant dimensionless velocity of 1, the wave is propagated from the inlet side, or left side in this case, through the contact area. In order to fully comprehend this behavior and verify the algorithm, pseudo-interferometry graphics of the film thickness were obtained. Fig. 7 shows clearly a wave propagating, from the inlet region, across the contact area. Similar results are found in [9].

Having achieved a good transient response for the EHL contact algorithm, the mutual approach variable H_0 is now treated as the principal direction of the dynamic contact system. Therefore Eq. (7) is applicable to this case. It is important

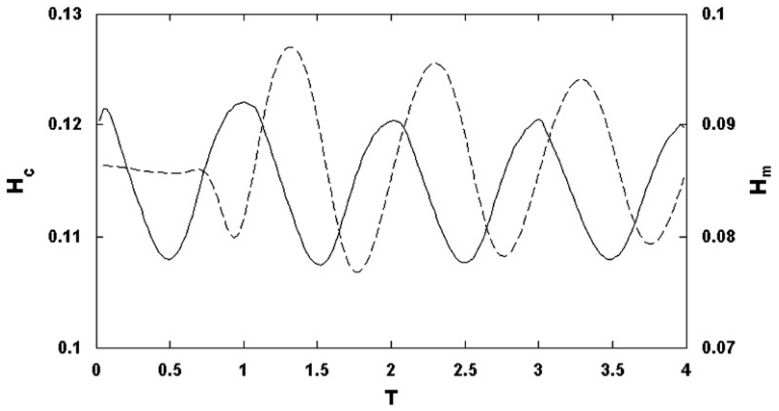

Fig. 6. Transient minimal, H_m(—), and central, H_c(– –), film thickness for M=200, L=10 and Ω_n=513.

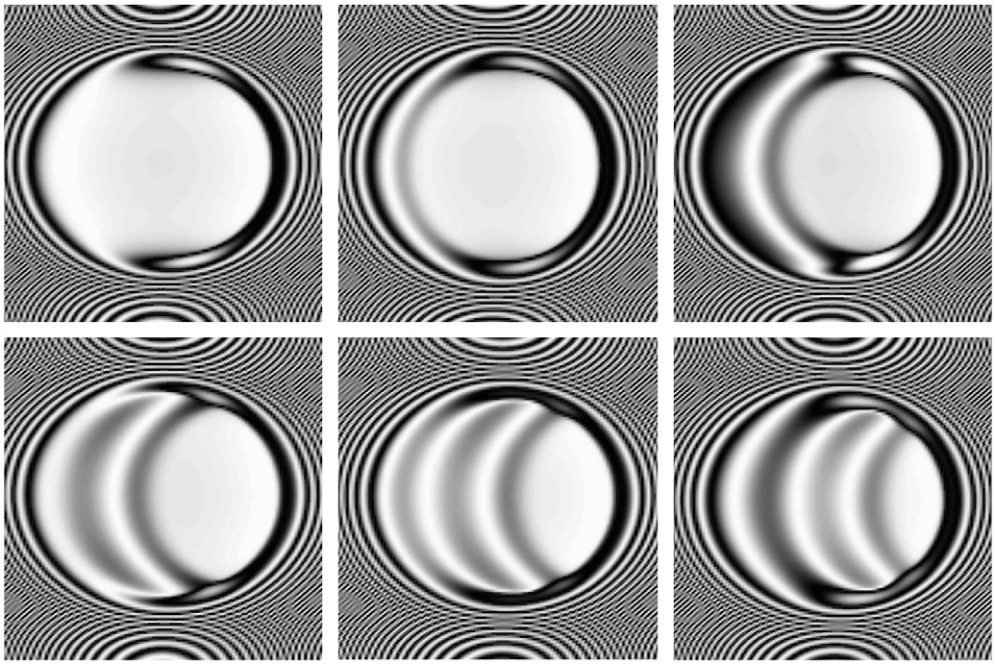

Fig. 7. Pseudo-interferometry fringes for the EHL contact of Fig. 3, starting at T=0.0 with ΔT=0.25 between pictures.

Table 1
Fitted coefficient values for three different natural frequency cases.

Case	M	L	κ	Ω_n	K_1	C_1	e_f	e_{ii}
1	200	10	0.5	10.26	1.1521	0.01037	1.1623E-03	6.2361E-01
2	200	10	0.5	5.13	1.1519	0.01238	7.0616E-04	9.2056E-01
3	200	10	0.5	2.56	1.1507	0.01034	2.5072E-04	6.1221E-01

to note that the value for the mutual approach differs from the minimal or the central film thickness, being a constant value across all contact area and a good way to evaluate the system's dynamic.

At first the two cases presented in Fig. 5 were evaluated. The fitting procedure took place using the least-squares method outlined before, where the mutual approach is handled as the displacement on Eq. (7) and the velocities attained from the dynamic EHL algorithm. Also, in order to evaluate the linear system given in Eq. (10), at each integration step there should be an integration of the pressure field over the domain, to obtain the EHL dynamic force. The results from the linear fit are listed in Table 1.

Also in Table 1, a measure of the error on the fitting process had to be introduced with the aim of performance control. For these cases, a point-wise difference method was employed. For every discrete point, its difference towards the valued to be fitted is summed, producing an overall error value for the fitted interval. Eq. (13) shows the general fitting error expression used.

$$e_v = \frac{\sum_i v_i - v_i^*}{\sum_i v_i} \tag{13}$$

where v denotes the evaluated variable and v^* the fitted values for such variable. Further on, it will be seen that just one global error for the mutual approach is not enough to represent the fitting procedure. Despite the low error values for the least square method and the rather good constancy on the fitting of the coefficients, the plotted curves showed some deviation from the original results.

For all three cases, an amplitude deviation can be noticed on the force adjustment. Fig. 8 shows exactly this effect. Moreover using the fitted coefficient values to obtain the acceleration of the system by isolating $\ddot{u} = d^2H_0/dT^2$ from Eq. (7), another fitting precision measurement can be done. However, the same amplitude problem is observed.

Despite previous results in this area, the linear dynamic model for the EHL contact seams not to fully represent the EHL contact behavior. Even though, it is a fairly good approximation to the system. However, in order to overcome this problem, a non-linear dynamic model as given before can be used. By means of Eq. (11), there are now seven dynamic coefficients to be adjusted to the force curve. Most of these coefficients have no physical meaning, whatsoever. Nevertheless, they represent a unique stiffness and damping polynomial, with a specific behavior.

Still, even without tangible meaning, these polynomials have to represent equally the behavior of a given system, thus having no modifications of its results when, for instance, the suspended mass is increased, but Moes' parameters are maintained constant. In other words, even with a change in the boundary conditions, the EHL system dynamic characteristics have to be regarded as unchanged. Therefore, the same system, as given in Table 1, (M=200, L=10 and κ=0.5), with three different natural frequencies, i.e., three different suspended masses, was evaluated by means of the nonlinear system of Eq. (12).

A sensitivity analysis was made, in order to reduce the total number of dynamic coefficients, decreasing the fitted polynomial complexity, as in Nonato [19]. The sensitivity analysis was carried on removing one coefficient at a time from the nonlinear system; and the residuals from the fitting procedure compared as in Table 2. As it can be observed, using only the linear damping coefficient, i.e., a viscous damper is enough to represent the damping due to the oil film. However, the stiffness is not enough represented when using less than three coefficients. Therefore, the stiffness is a third order polynomial.

Hence, using coefficients K_1, K_2 and K_3 for the stiffness and C_1 for the damping, the EHL dynamic contact is fully represented by a nonlinear spring and a viscous damping model. The new dynamic coefficients are listed in Table 3.

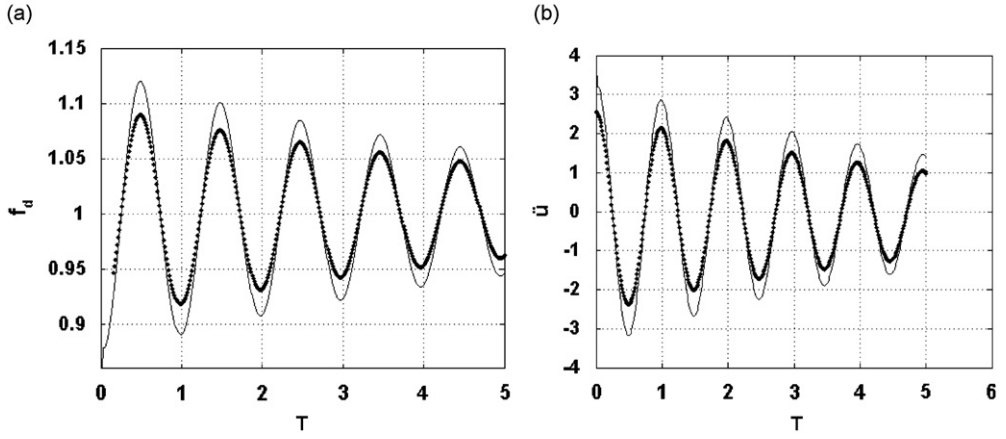

Fig. 8. Simulated (—) and fitted results (•) for the (a) EHL dynamic force, f_d, and (b) system acceleration, $\ddot{u}$, using the linear dynamic model for case 2.

Table 2
Residuals from the sensitivity analysis.

Coef.	All	$-K_1$	$-C_1$	$-K_2$	$-C_2$	$-K_3$	$-C_3$	$-B_4$
e_f	4.059E-08	3.197E-05	4.417E-08	6.803E-07	5.978E-08	1.921E-06	4.379E-08	4.602E-08
$e_{\ddot{u}}$	2.711E-05	1.621E-02	2.956E-05	4.490E-04	3.806E-05	1.218E-03	2.937E-05	3.121E-05

Table 3
Fitted non-linear coefficients values and fitting residuals for three different natural frequency cases, with M=200, L=10 and κ=0.5.

Case	Ω_n	K_1	K_2	K_3	C_1	e_f	$e_{\ddot{u}}$
1	10.26	1.552	−1.414	1.093	0.011	−9.987E-10	2.255E-06
2	5.13	0.806	0.346	0.054	0.013	1.094E-08	−1.253E-05
3	2.56	0.747	0.502	−0.046	0.015	8.897E-09	1.830E-04

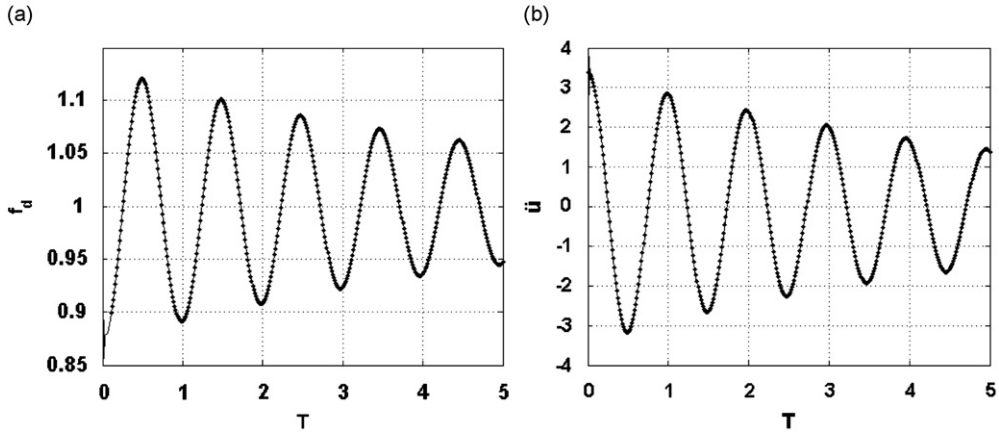

Fig. 9. Simulated (—) and fitted results (●) for the (a) EHL dynamic force, f_d, and (b) system acceleration, $\ddot{u}$, using the non-linear dynamic model for case 2.

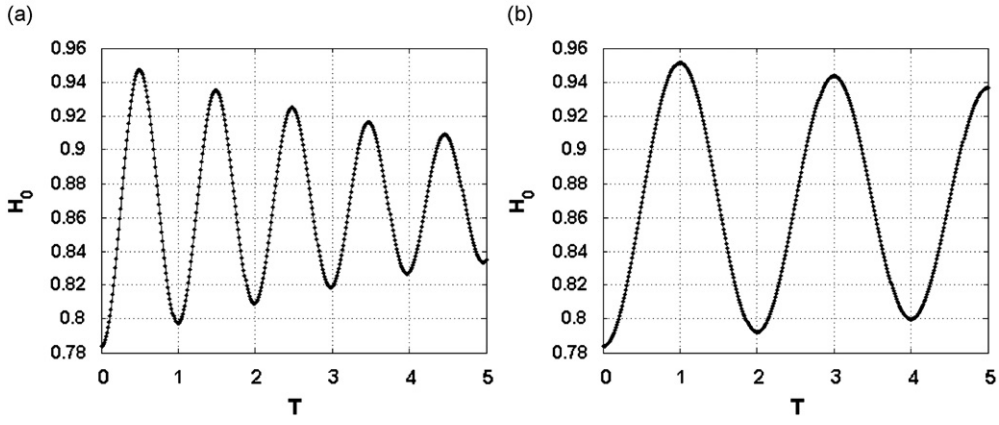

Fig. 10. Simulated (—) and fitted results (●) for the EHL contact mutual approach for (a) case 2 and (b) case 3, using the non-linear dynamic model.

With this nonlinear dynamic system, the EHL dynamic contact should have a better cohesion between the simulated and fitted data graphics. In Fig. 9, the same cases shown in Fig. 8 are represented using the new nonlinear approach. As anticipated by the lower residuals found, both curves have almost the same behavior, without the amplitude errors as seen before.

The adjustment level of the nonlinear system to the dynamic EHL contact is now greatly increased. Therefore, one is now capable of reproducing the displacement response, as in Fig. 5, through a nonlinear spring and a viscous damping model. For that, a modified Runge–Kutta integrator of second and third orders was used to integrate the motion equation of the spring and damper model. Fig. 10 shows the fitted values of displacement to the mutual approach obtained from the EHL dynamic algorithm.

Having achieved an adequate fitting method for the EHL dynamic contact system, further investigations are possible. Previous methods, as presented in Wijnant [9] and Wijnant and Wensing [11], had a better linear approximation; however its fitting procedures were made upon the harmonic results, as pointed out before, and presented, then, a greater complexity. To confirm the non-linearity of the EHL contact, the harmonic response was also evaluated using the least-squares fitting procedure.

One of the first hypotheses made on the harmonic response model was that the suspended mass has low or no effect on the complete system dynamic. Hence, the inertia term of the motion equation vanishes, making the analysis a quasi-static procedure. The fact is trustworthy when dealing with low masses and, therefore, high natural frequencies. In this case, one might say that the exciting frequency is dominant over the free vibrations and the natural frequency does not play a big role in the contact response.

The results expected from the harmonic quasi-static algorithm, however, should not have different behavior from those of the free vibration for the same dynamic system, i.e., for the same EHL contact system, the stiffness should have the same nonlinearity as presented in free vibration, and the damping would also be viscous. For this reason, the same analysis applied to the free vibration results were made upon the harmonic excitation cases.

Initially, in order to check the proper behavior of the harmonic response, the mutual approach for two different exciting frequencies, over the same contact case of the free vibration, is shown in Fig. 11. As expected, the mutual approach for the exciting frequencies $\Omega_e=\pi$ and $\Omega_e=2\pi$ have, respectively, the periods 2.0 and 1.0 approximately. Also the wave propagation phenomena can be seen on the results.

Fig. 12 shows the pseudo-interferometry fringes for $T=0.0$, $T=0.5$ and $T=1.0$. Therefore, the harmonic excitation algorithm also returned fine results and could be used on the fitting procedures.

The linear fitting method was then applied to the harmonic results. Differently from the free vibration model, where the motion equation is also evaluated along with the EHL algorithm, the velocity of the contact system must be integrated from the mutual approach as no equation of motion exists for this case. As seen before, there is no need of great modifications on the fitting methods to employ it in the fitting procedure of the harmonic results. Consequently, there is no increase in the complexity of the method. The linear coefficients, so as the residuals from the fitting procedure are listed in Table 4.

Further references made to the EHL contact and loading cases will use the same numbers as given in Tables 1 and 4. Even having a smaller residual, the amplitude deviation is still present for these cases. In the harmonic fitting, there is no

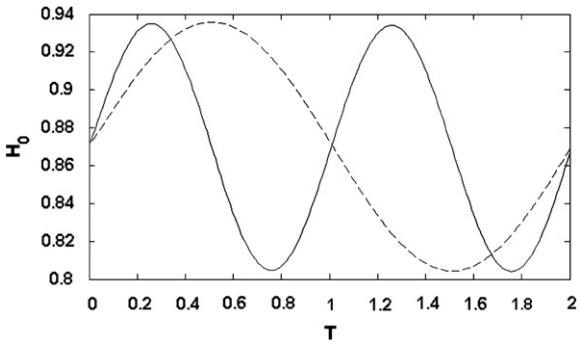

Fig. 11. Harmonic mutual approach response for EHL elliptic contact with $M=200$ and $L=10$ for two different exciting frequencies, $\Omega_e=\pi$ (– –) and $\Omega_e=2\pi$ (—).

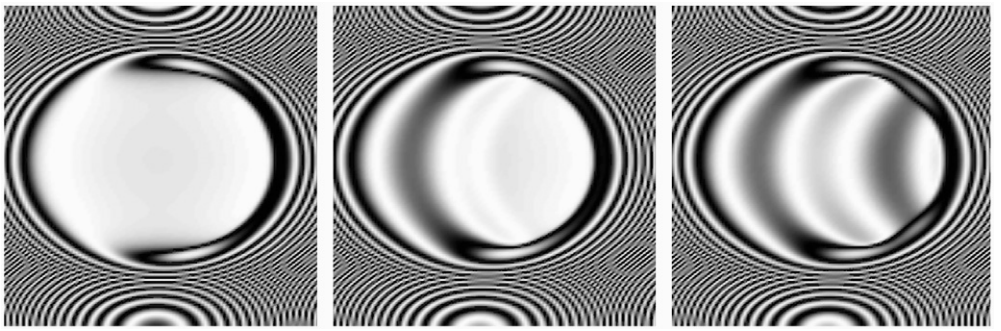

Fig. 12. Pseudo-interferometry fringes for the EHL contact of Fig. 8 with $\Omega_e=2\pi$, for $T=0.0$, 1.0 and 2.0.

Table 4
Fitted coefficient values for three different excitation frequency cases.

Case	M	L	κ	Ω_e	K_1	C_1	e_f
4	200	10	0.5	π	1.1511	0.02521	8.8713E-04
5	200	10	0.5	2π	1.1540	0.01381	9.1113E-04
6	200	10	0.5	4π	1.1519	0.01247	9.3445E-04

meaning of using acceleration residuals, as there was no acceleration calculation from the algorithm itself. Therefore, the analysis only regards the force residuals. Fig. 13 presents the fitted data and the simulated EHL dynamic force.

In order to avoid the same fitting deviations, as in the free vibration cases, the non-linear method was also employed. Using the same third order polynomial fit for the stiffness and the viscous damping, new coefficients were obtained, now for the harmonic responses. Table 5 lists these new coefficients.

Even without a closer resemblance between the free vibration results and even between the results from cases 4–6, the fitting procedure achieved good correspondence, as shown in Fig. 14. Also, Fig. 15 presents the integrated mutual approach from the nonlinear model compared to the simulated results. The fitting results clearly show the increased precision of the method, when compared with the linear one.

However, regarding the fitted coefficients, one might conclude that for the same contact system, i.e., the same M, L and κ, the harmonic and free vibration gave different results. Furthermore, for the harmonic responses, the method herein has a low consistency. Even though, the authors draw the reader attention to the nature of the fitting procedure itself.

Using third order polynomials to represent the stiffness curves, through a least-square method, can produce some variation of the results. The least square method only provides the best fitted polynomial to the evaluated interval; therefore, several polynomials can describe the stiffness behavior of the EHL contact in this region, but differ in results outside the range. It can be observed in Fig. 16, where the graphic shows the polynomial fitted over the evaluated range of H_0 and outside the region.

The predicted values for the spring force around 1 are similar for all three polynomials. Therefore, the three polynomials can be used to predict the mutual approach for the EHL contact described before, as its values would not diverge much

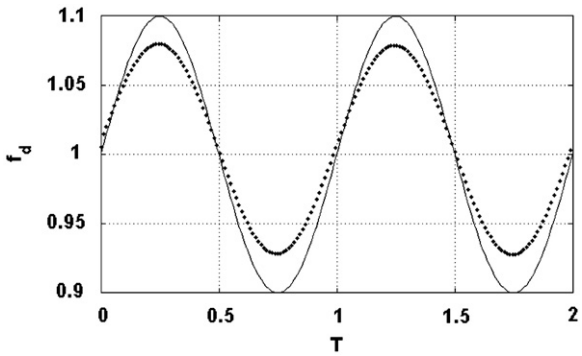

Fig. 13. Simulated (—) and fitted results (•) for the EHL dynamic force, f_d, using the linear dynamic model for case 5.

Table 5
Fitted non-linear coefficients values and fitting residuals for three different excitation frequency cases, where M=200, L=10 and κ=0.5.

Case	Ω_e	K_1	K_2	K_3	C_1	e_f
4	π	0.703	0.596	−0.097	0.015	4.17E-09
5	2π	0.603	0.815	−0.215	0.013	2.31E-09
6	4π	0.413	1.236	−0.444	0.011	−9.93E-10

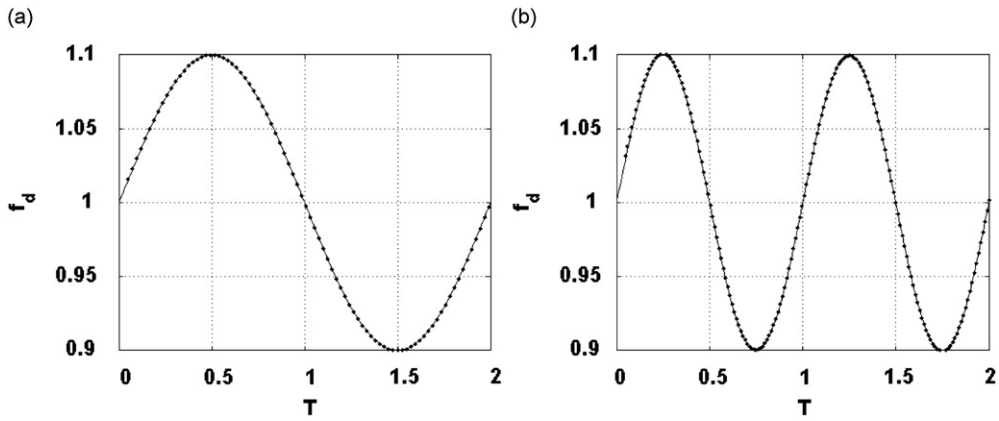

Fig. 14. Simulated (—) and fitted results (•) for the EHL dynamic force, f_d, using the non-linear dynamic model for (a) case 4 and (b) case 5.

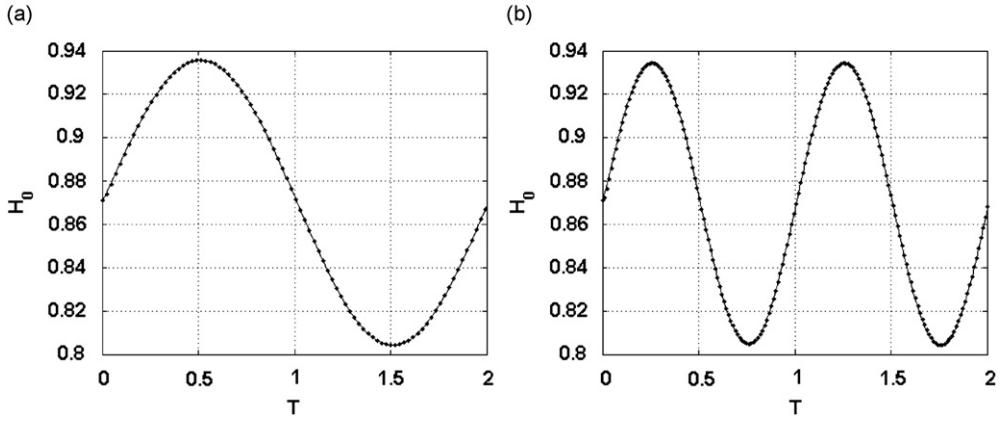

Fig. 15. Simulated (—) and fitted results (•) for the EHL contact mutual approach using the non-linear dynamic model for (a) case 4 and (b) case 5.

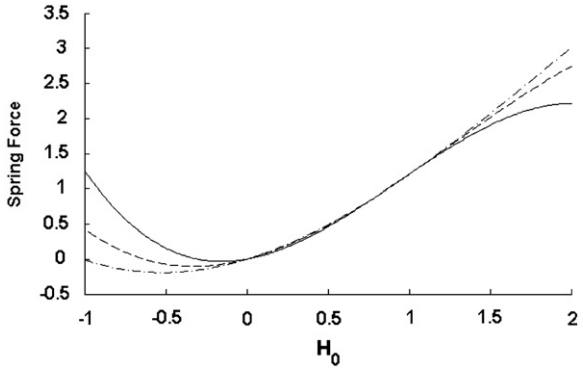

Fig. 16. Stiffness polynomials for case 4 (– • –), case 5(– –) and case 6(—).

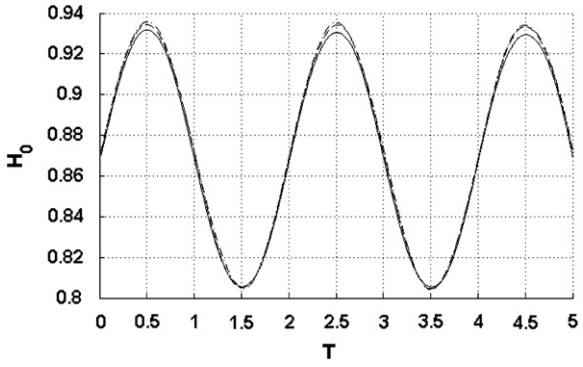

Fig. 17. Mutual approach for the non-linear dynamic models of case 4 (– • –), case 5(– –) and case 6(—).

from one to another. Using these polynomials, the nonlinear dynamic system can be modeled for one specific case. Fig. 17 shows the mutual approach simulated for the EHL contact (M=200, L=10 and κ=0.5), with an exciting frequency of $\Omega_e=\pi$.

The same analysis can be made for the free vibration cases 1, 2 and 3. Fig. 18 shows the three dynamic models of Table 3, for a system with Ω_n=2.56. As it can be seen, even with some difference in the polynomials coefficients, all dynamic systems have almost the same behavior over the simulated mutual approach range and they can satisfactorily represent the EHL contact.

Once verified the nonlinear model for the free vibration and harmonic loading cases, one might use its results to an EHL contact with different loading condition and expect the same level of correlation. Having the results from the validation of the algorithm, which depicted the contact response to a ramp loading, the fitting procedure is also applicable. Fig. 19 shows

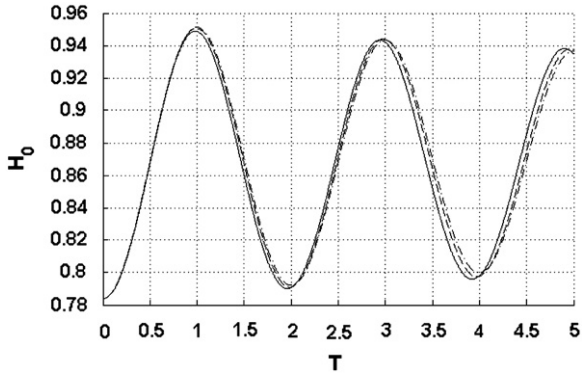

Fig. 18. Mutual approach for the non-linear dynamic models of case 3 (– ● –), case 2(– –) and case 1(—).

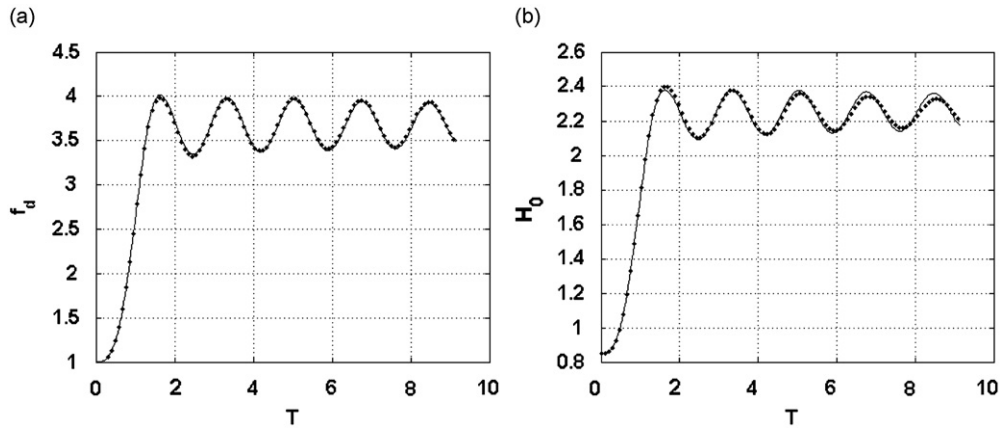

Fig. 19. Simulated (—) and fitted results (●) for the (a) EHL dynamic force, f_d, and (b) mutual approach, H_0, for the validation model results.

Table 6
Fitted coefficients from the nonlinear model for the algorithm response of the experimental validation case.

Case	Ω_n	K_1	K_2	K_3	C_1
Validation	2.4	0.8674	0.3823	−0.0185	0.033

the fitted results for contact force and mutual approach compared to the simulated validation case. Also the adjusted coefficients are listed in Table 6. The obtained correlation shows to be rather consistent between fitted and simulated data.

Any inconsistence of the nonlinear contact stiffness model should be noticeable, once the increase in load is transient and uncertainties of the practice results become much clearer. That is, the increase in load was not modeled as a stepwise increase in the actual load, which complies with a much simpler approach. In this case, all the transient effects of the contact are present in the response and the fitting method was able to represent them.

5. Conclusion

The proposed non-linear dynamic model for EHL contacts has shown to be feasible and of simple implementation. The achieved results revealed a good cohesion to the simulated model. Previous approaches, as the linear ones, still have application in this field; however, as presented here, the non-linear model is considerably a most precise one. Even for the results obtained for the experimental data, the nonlinear model still covers all peculiarities of the EHL contact.

Having the EHL transient responses, it is easily possible to verify the conditions for the non-linear dynamic model, and apply the results on the system, making the EHL contact a flexible linkage between the contact parts. The model suggested here is applicable to any lubricated contact or dynamic system with one degree of freedom and can be expanded for higher order systems.

However, further investigation on the actual behavior of each dynamic system is required. The validity of the results for the EHL contact are supported by previous experimental results obtained in this specific matter. However, little is the

knowledge from its dynamic characterization. The use of the results presented here in mechanical components, such as rolling elements bearings, regarded as a full system, is straightforward and can be a suitable validation method.

Acknowledgements

The authors thank FAPESP, CNPq and SHAEFFLER BRASIL company for the support of this research.

References

[1] C.V.S. Villa, J. Sinou, F. Thouverez, Investigation of a rotor-bearing system with bearing clearances and Hertz Contact by using a harmonic balance method, *Journal of the Brazilian Society of Mechanical Science and Engineering* 29 (1) (2007) 14–20.
[2] Hamrock, Bernard. J., Isothermal elastohydrodynamic lubrication of point contacts, Leeds, Inglaterra: Leeds University, (1976) 256p. Thesis (Ph.D.).
[3] H.P. Evans, R.W. Snidle, Inverse solution of Reynolds' equation of Lubricatio under point-contact elastohydrodynamic conditions, *ASME Journal of Tribology* 103 (1981) 539–546.
[4] H.P. Evans, R.W. Snidle, The isothermal elastohydrodynamic lubrication of spheres, *ASME Journal of Tribology* 103 (1981) 547–557.
[5] T. Park, K. Kym, A numerical analysis of the elastohydrodynamic lubrication of elliptical contacts, *Wear* 136 (1990) 299–312.
[6] C.H. Venner, A.A. Lubrecht, *Multilevel Methods in Lubrication*, vol. 37, Elsevier, Tribology Series, Netherlands, 2001 400p.
[7] C.H. Venner, A.A. Ludbrecht, Numerical simulation of a transverse ridge in a circular EHL contact under rolling/sliding, *ASME Journal of Tribology* 116 (1994) 751–761.
[8] C.H. Venner, A.A. Ludbrecht, Numerical analysis of the influence of waviness on the film thickness of a circular EHL contact, *ASME Journal of Tribology* 118 (1996) 153–161.
[9] Ysbrand Hans, Wijnant, Contact dynamics in the field of elastohydrodynamic lubrication, Enschede, the Netherlands: University of Twente, (1998) (179p) Thesis (Ph.D.).
[10] Jeroen Anton, Wensing, On the dynamics of ball bearings, Enschede, the Netherlands: University of Twente, (1998) 173p Thesis (Ph.D.).
[11] Y.H. Wijnant, J.A. Wensing, G.C. vanNijen, The influence of lubrication on the dynamic behaviour of ball bearings, *Journal of Sound and Vibration* 222 (4) (1999) 579–596.
[12] C.E.,Goodyer; Adaptive numerical methods for elastohydrodynamic lubrication, Leeds, England: University of Leeds, (2001) (179p), Thesis (Ph.D.).
[13] F., Nonato, K.L., Cavalca, Nonlinear dynamic model for transient elastohydrodynamic contact forces, in: Proceedings of the COBEM 2009—20th International Congress of Mechanical Engineering, (2009) 9p.
[14] D. Dowson, G.R. Higginson, in: *Elasto-hydrodynamic Lubrication—SI Edition*, first ed., Pergamon Press, Great Britain, 1977.
[15] R., Larsson, P.O., Larsson, E., Eriksson, M., Sjöberg, E., Höglung, Lubricant properties for input to hydrodynamic and elastohydrodynamic lubrication analyses, in: IMechE 2000, Proceedings of the Institution of Mechanical Engineers, vol. 214, (J) 17–27.
[16] S.X. Zhao, X.D. Dai, G. Meng, J. Zhu, An experimental study of nonlinear oil-film forces of a journal bearing, *Journal of Sound and Vibration* 287 (2005) 827–843.
[17] H. Zhou, S.X. Zhao, H. Xu, J. Zhu, An experimental study on oil-film dynamic coefficients, *Tribology International* 37 (2004) 245–253.
[18] H.F., Castro, K.L., Cavalca, Non-linear hydrodynamic bearing force characterization under fluid-induced instability, in: DINAME 2009, Proceedings of the XII International Symposium on Dynamic Problems of Mechanics, 10p. (2009).
[19] Fábio de Paula Nonato, in: *Dynamic Model for the Contact in Rolling Element Bearings under Elastohydrodynamic Lubrication*, University of Campinas, Campinas, Brazil, 2009 130p., (Portuguese), Dissertation (Master Degree).
[20] H. Moes, Optimum similarity analysis with applications to elastohydrodynamic lubrication, *Wear* 159 (1992) 57–66.
[21] N. Ren, D. Zhu, S.Z. Wen, Experimental method for quantitative analysis of transient EHL, *Tribology International* 24 (04) (1991) 225–230.
[22] J.P., Chaomleffel, G., Dalmaz, P., Vergne; Experimental results and analytical predictions of EHL film thickness, in: Proceedings of the 33rd Leeds Lyon Symposium on Tribology, Leeds—United Kingdom, (2006).
[23] C.W., Chang-Jiang, C.K., Chen; Non-linear dynamic analysis of bearing-rotor system lubricating with couple stress fluid, in: IMechE 2008, Proceedings of the Institution of Mechanical Engineers, vol. 222, (C), 599–616, (2008).